Proceedings of ASME Turbo Expo 2020
Turbomachinery Technical Conference and Exposition
GT2020
September 21-25, Virtual, Online

GT2020-14893

CHARACTERISING HYDROGEN MICROMIX FLAMES: COMBUSTION MODEL CALIBRATION AND EVALUATION

Marcos López-Juárez[1], Xiaoxiao Sun[*1], Bobby Sethi[1], Pierre Gauthier[2], David Abbott[1]

[1]School of Aerospace, Transport and Manufacturing, Cranfield University,
College Road, Cranfield, MK43 0AL, United Kingdom
[2]Siemens Canada Limited,
9545 Cote de Liesse Road, Montreal QC H9P 1A5, Canada

ABSTRACT

Hydrogen micromix combustion is a promising concept to reduce the environmental impact of both aero and land-based gas turbines by delivering carbon-free and ultra-low-NO_x combustion without the risk of autoignition or flashback. The ENABLEH2 project aims to demonstrate the feasibility of such a switch to hydrogen for civil aviation, within which the micromix combustion, as a key enabling technology, will be matured to TRL3. The micromix combustor comprises thousands of small diffusion flames for which air and fuel are mixed in a cross-flow pattern. This technology is based on the idea of minimizing the scale of mixing to maximize mixing intensity. The high-reactivity and wide flammability limits of hydrogen in a micromix combustor can produce short and low-temperature small diffusion flames in lean overall equivalence ratios.

For hydrogen-air mixtures there is a need to further characterise the physical importance and calibration process of the laminar Schmidt (Sc), Lewis (Le) and Prandtl (Pr) and turbulent Schmidt (Sc) numbers. In addition, there is limited numerical and experimental data about flame characteristics and emissions of hydrogen micromix combustor at high pressure and temperature conditions.

In this paper, the CFD software STAR-CCM+ was used with the FGM (Kinetic Rate) combustion model to simulate and calibrate hydrogen micromix flames. The research was divided into two parts. In the first part, the values of laminar Schmidt, Lewis and Prandtl numbers for H_2 and air, non-reactive, flow mixtures were estimated as 0.22, 0.3 and 0.75 from correlations obtained in the literature. The typical Borghi diagram has been modified to represent this type of diffusion flame, since the assumption of Sc = Le = Pr = 1 can not be applied to hydrogen micromix flames and it is only for premixed flames. This diagram characterizes flame regime based on Damköhler (Da), Karlovitz (Ka) and turbulent Reynolds (Ret) numbers that were calculated from preliminary CFD simulations.

In the second part, the value of laminar Schmidt number was set as constant while laminar Lewis and Prandtl numbers were obtained from the flamelet tables. A Turbulent Schmidt number was then obtained by comparing RANS and LES simulations of a single injector. If Sc_t>0.2, the predicted NO_x production of RANS simulations approaches that of LES; while Sc_t<0.2 provides similar overall flame structure between RANS and LES. It is concluded that, for the current simulations, Sc_t=0.2 is a good compromise between flame structure and emissions prediction. Flame characteristics and NO_x emissions given by Thickened Flame and FGM Kinetic Rate models in a single injector geometry were also compared.

Keywords: Hydrogen; Micromix; Combustion; Calibration; ENABLEH2; STAR-CCM+; FGM Kinetic rate; Thickened Flame.

NOMENCLATURE

α	thermal diffusivity
$D_{i/j}$	molecular diffusivity of i in j
Da	Damkohler number
δ_l	laminar flame thickness
ϕ	equivalence ratio
k	thermal conductivity
Ka	Karlovitz number
Le	Lewis number
ν	kinematic viscosity
μ	dynamic viscosity
μ^d	dilute dynamic viscosity
μ^r	residual fluid dynamic viscosity
p	static pressure

[*] Address all correspondence to this author: x.sun@cranfield.ac.uk

p_0	total pressure
Pr	Prandt number
Re_t	turbulent Reynolds number
Sc	Schmidt number
S_l	laminar flame speed
ρ	density
T	static temperature
T_0	total temperature
T_b	burned gases temperature
T_u	unburned gases temperature
u'	turbulent (fluctuating) speed
Z	mixture fraction
z	compressibility factor

INTRODUCTION

The aerospace sector, as well as the automotive sector, is under the most restrictive anti-emissions law in history and these low-emission requirements are going to be further increased as time goes by. For the aerospace industry, CO2 and NO_x are mainly the emissions that must be mitigated. In order to make it possible, the European programs Vision 2020 and Flightpath 2050 aim to reduce these emissions by setting goals and funding projects to achieve them. The goals target a reduction of CO_2 and NO_x emissions by 50% and 80% in 2020 and by 75% and 90% in 2050 respectively relative to 2000 levels [1, 2]. In contrast, according to ICAO, with the current growing trend of the civil aerospace sector, CO_2 emissions are expected to increase [3]. This is clearly a fact that goes against EU objectives and must be addressed urgently since the aviation sector is responsible for roughly the 5% of man-made global warming [4].

At this point, a clear conclusion can be extracted: even with more electric propulsion, EU objectives are very challenging and might not be fulfilled. In this situation, alternative fuels such as hydrogen may be part of the solution

Hydrogen is proposed as fuel not only because its combustion does not produce carbon emissions but also because of its high reactivity. This property has mainly two consequences that tend to reduce NO_x production. Hydrogen flames is charaterised by lower residence time therefore lower NOx. Hydrogen is able to burn at much leaner equivalence ratio than kerosene [5, 6], which potentially reduces local flame temperatures. However, if fuel-to-air mixing is not adequate, its high calorific value leads to higher flame temperature at stoichiometry, increasing NO_x production.

Since H_2 properties are very different from hydrocarbon fuel (mainly higher reactivity, diffusivity and calorific power [7]), a conventional combustion system is not suitable for air-to-hydrogen mixing. If it is used in a conventional combustion chamber, relatively high equivalence ratio regions are produced hence slightly higher NO_x emissions than kerosene combustion are generated [6].

Micromix combustion system allows to make use of the full potential of hydrogen combustion by reducing significantly NO_x emissions. This technology was developed based on the idea of minimizing the scale of mixing to maximize the mixing intensity [6]. In order to do that, a micromix combustor is composed of thousands of small cross-flow injectors. By this way, for a given point of operation, the amount of fuel required is distributed among numerous orifices ensuring lean diffusion combustion in short flames, thus reducing high local temperatures and residence time hence NO_x production.

Recently, ENABLEH2 project [9] was launched in order to develop this technology to meet emission targets for 2050. The aim of this project is to mature LH_2-based propulsion technologies to TRL4 to enable free-CO_2 and ultra-low-NO_x engines in the future. This paper is part of the research carried out by Cranfield University in ENABLEH2 project.

Developing technology to TRL4 means to create a system/subsystem model or prototype demonstrator in a relevant environment [10]. Fortunately, nowadays CFD software tools are very powerful and are used extensively in industry. In order to raise the TRL of a technology whose physics have been understood but not accurately predictable in any operating condition, validation of CFD models is a necessary step for future optimization of the technology. In this paper, preliminary analyses were carried out to stablish best practices for CFD modelling of H_2/air cross-flow combustion. Validation of CFD simulations will be performed in the following years with the experimental data that will be generated by Cranfield University as part of ENABLEH2 project.

The high diffusivity of H_2 makes the mixing characteristics of any H_2/air mixture different from those of any hydrocarbon/air mixture. Therefore, the molecular properties of the mixture are different as well. These fluid characteristics are usually expressed by means of the Lewis (Le), Schmidt (Sc) and Prandtl (Pr) numbers. For CFD simulations, knowing the value of these numbers is critical to implement the molecular properties of the fluid in the simulations. However, in the literature there is a lack of information about the value of these parameters at different temperatures, pressures and equivalence ratios. In this paper, the basic guidelines to obtain these numbers from correlations and their values for a wide range of temperatures, pressures and equivalence ratios are provided.

In RANS simulations, the mixing produced by turbulence is modelled through the turbulent Schmidt number (Sc_t). This parameter only depends on the flow characteristic and has been estimated as 0.2 in simulations for non-reactive cross-flow patterns [11]. However, the changes in the flow pattern produced by combustion and their subsequent effect on Sc_t have not been assessed. The value of this number was re-evaluated for H_2-micromix flames.

The flame regime defines the turbulence-chemistry interactions for any flame. In any simulation, knowing the flame regime is critical in order to choose the CFD combustion models since they define the chemistry and the turbulence-chemistry interactions. In the literature, the Borghi diagram has been extensively used for almost any type of flame regardless of the fuel. However, using it with H_2-micromix diffusion flames is not justified because it implicitly assumes $Sc = Le = Pr = 1$ and should only be used for pre-mixed flames. Since Sc, Le and Pr for H_2-micromix flames differ from 1 and they are diffusion

flames, a new flame diagram was proposed to stablish the flame regime and preliminarily choose the CFD combustion models.

In order to model combustion, Flamelet Generated Manifold (FGM) and Thickened Flame models seem to be promising. FGM model has been used during last decades providing good predicting capabilities for solving hydrocarbon and hydrogen combustion [12, 13, 14, 15, 16]. The flamelet model generates beforehand tabulated values for the combustion. Thenthese flamelets are integrated in the actual simulation by using the progress variable and the mixture fraction parameters, computed from their corresponding transport equation. Tabulated values calculated prior to the simulation decouples chemistry with flow simulations hence reduce considerably the computational cost of solving the combustion phenomenon [12]. Thickened flame model, used only for LES simulations, has been recently used as a promising model to calculate flame physics at sub-grid scale with relatively coarse mesh. This is achieved by artificially thickening the flame front to solve it in detail while keeping constant laminar flame speed [17, 18]. The results provided using these two models were compared to provide a deeper insight on the different possibilities to model this type of flames.

Along this paper, a know-how about the calibration and model-selection process for H_2-micromix combustion simulation is provided.

1 Physics of H_2/air mixtures

The first step before running any numerical study is to identify the physics behind it in the range of p and T that are going to be simulated. This could be done by estimating the molecular and turbulent properties of the working fluid and the expected value for the interest variables. For this it is necessary to conduct a thorough literature review to get correlations and mixing models that can describe the fluid and flow field properties. This task is especially important in hydrogen-fueled cross-flow combustion since most of the work done for combustion is usually related to hydrocarbon fuels in other types flow field such as the toroidal recirculation vortex in conventional combustion chambers.

Regarding the properties of the fluid, the usual way of characterizing them is through the Schmidt (Sc), Lewis (Le) and Prandt (Pr) numbers:

$$Sc = \frac{\nu}{D}; \quad Le = \frac{\alpha}{D}; \quad Pr = \frac{\nu}{\alpha}; \tag{1}$$

Traditionally, the value of these parameters was assumed 1 for hydrocarbon-fueled combustion. However, this is not correct when the fuel is hydrogen, since its high molecular diffusivity implies lower-than-1 Le and Sc numbers. Due to the relevance of the molecular and thermal diffusivities in the mixing process and flame structure of any combustion system, these non-dimensional numbers must be known for all the operating conditions.

The molecular properties that are required to obtain these parameters are the dynamic viscosity (μ), the density (ρ), the compressibility factor (z), the thermal conductivity (k) and the isobaric specific heat (C_p). In this section the correlations that were used to calculate these properties are referenced and the values of the Sc, Le and Pr numbers for a wide range of pressures presented.

1.1 Dynamic viscosity

Lemmon et al. [19] developed a correlation to calculate the dynamic viscosity of air and validated it with REFPROP 7.0 database. All the predicted values fall within a ±5% of error for $T \in [100, 1000]\, K$ and $p \in [1, 1200]\, bar$.

Yusibani et al. [20] developed a similar correlation to predict the dynamic viscosity of H_2 valid in the range of $T \in [100, 1000]\, K$ and $p \in [1, 2200]\, bar$ with a maximum error of ±4% validated with experimental results.

In both correlations the dynamic viscosity is calculated as $\mu = \mu^d + \mu^r$, where μ^d is the dilute dynamic viscosity (independent of pressure) and μ^r the residual fluid viscosity (representing the effect of pressure).

1.2 Density and compressibility factor

These two parameters are calculated together. First, correlations and data from tables are used to calculate the compressibility factor. Finally, this parameter is used in the ideal gas law to calculate density (1).

$$\rho = \frac{p}{zRT} \tag{2}$$

The compressibility factor of air is obtained from linear interpolation in pressure and temperature from experimental data obtained from *Perry's chemical engineers' handbook* [21]. The range of validity for this correlation is $T \in [75,1000]\, K$ and $p \in [1,500]\, bar$. The uncertainty of using this data is unknown.

To calculate the compressibility factor of hydrogen, Lemmon et al [22] develop d a simple correlation based on experimental results provided by the software REFPROP. Their method is valid in the range of $T \in [200,1000]\, K$ and $p \in [1,1200]$ bar with a maximum error around ±0.01%.

1.3 Thermal conductivity

Air thermal conductivity was also correlated by Lemmon et al. [19] with a formulation similar to the one used for dynamic viscosity with an additional term that includes the enhancement of thermal conductivity near critical conditions. This correlation is valid in the range of $T \in [100, 1000]\, K$ and $p \in [1, 1200]\, bar$ with an uncertainty lower than ±5% compared with experimental results.

The correlation developed by Assael et al. [32] to estimate the thermal conductivity of H_2 was used. It has an uncertainty lower than ±7% in the range of $T \in [100, 1000]\, K$ and $p \in [1, 1000]\, bar$ compared to experimental results.

1.4 Isobaric Specific Heat

Isobaric specific heat was considered to be independent of pressure. In order to get its evolution with temperature, the correlations found in the book *An Introduction to Combustion Concepts and Applications* [24] are used. H_2 specific heat is directly obtained from these correlations while for air, N_2 and O_2 specific heats are first obtained and then a weighted average value is calculated using the mass fractions.

1.5 Molecular Diffusivity

Molecular diffusivity describes how two or more fluids mix without the presence of a forced convection field according to the Fick's law. Since H_2 is the lowest concentration species that diffuses into air before combustion (lean equivalence ratio), the molecular diffusivity coefficient (D) is taken as the binary diffusion coefficient of H_2 into air.

A pressure-and-temperature-dependent binary diffusion model to estimate $D_{H_2/air}$ is extracted from the book *Gas Transport in Solid Oxide Fuel* Cells [25]. This correlation is based on the kinetic theory of gases, which could induce some errors depending on the condition. The constant 0.00197 is different from that found in [25] (0.00186) since it has been adjusted to match the experimental data found in [26].

1.6 Mixture models

In order to know the averaged value of μ, k, C_p and ρ for any mixture at a given condition knowing these properties for each species individually, a mixture model is needed. They are based on experimental results and can be as simple as using a weighted average depending on the mole fraction or far more complex depending on the fluid property.

The process that was followed to calculate the properties of the mixture is to firstly obtain the temperature of the mixture by applying energy conservation, then the properties of air and H_2 separately at the corresponding temperature and a chosen pressure, finally to apply the mixture models.

The isobaric specific heat of the mixture is obtained when calculating the temperature through energy conservation as a weighted average of the specific heats of the different species using the mass fractions.

For both dynamic viscosity and thermal conductivity the Wilke's law of mixing, derived from the kinetic theory of gases, is extensively used and shows good agreement with experimental measurements [27].

Density is obtained from the partial pressures of each species and the ideal gas law. This is equivalent as a weighted average using the mole fractions.

1.7 Laminar Sc, Le and Pr numbers

After correlating all the fluid properties and applying the corresponding mixture models, the non-dimensional numbers were calculated. First, they were calculated for $T \in [200, 1000]\,K$, $p \in (1, 5, 10, 20)\,bar$ and $\phi = 0.5$ to see how they change with pressure and temperature for a given mixture (figure 1). Finally, they were calculated for $T \in [200,1000]\,K$, $\phi \in (0.3, 0.5, 1, 2)$ and $p = 10\,bar$ to get their variation with the equivalence ratio (figure 2).

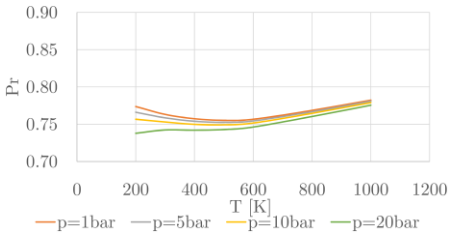

FIGURE 1: Evolution of Prandtl number with p and T at $\phi = 0.5$

According to the first calculation (constant ϕ), the fluid non-dimensional numbers are mostly insensitive to pressure and temperature in the studied range. The biggest variation, although not very significant, is observed in the Prandtl number (figure 1). This is because of the small variation in the dynamic viscosity and the thermal conductivity when only increasing pressure. In the case of the Schmidt number, the divergent isobaric lines at low temperature are due to the effect of the compressibility factor (since μ depends on ρ and $D_{H_2/air}$ on p, therefore z is not neglected). The insensitiveness of these parameters to p and T suggests that for a given equivalence ratio, assuming any of these parameters to be constant does not deviate too much from reality. However, the typical assumption of $Le = 1$ is indeed far from the actual physics, especially for H_2/air lean mixtures. For the leanest equivalence ratio (0.3) where NO_x are the lowest, the Schmidt, Lewis and Prandtl numbers are 0.22, 0.3 and 0.75 respectively.

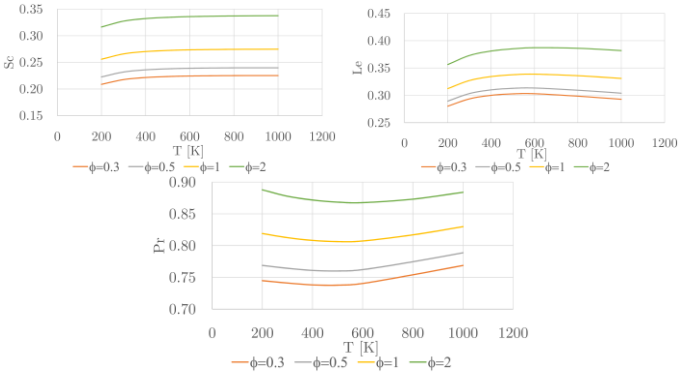

FIGURE 2: Evolution of Schmidt, Lewis and Prandtl number with ϕ and T at $p = 10\,bar$

If different mixtures of H_2 and air are considered, it is possible to find differences in the non-dimensional numbers. However, they do not change more than 0.15 when comparing lean and rich mixtures. *Le* takes as much a value of 0.4, still far from 1. The values of $\phi \in (0.3, 0.5, 1, 2)$ have been chosen to be those that could represent a diffusion flame behaviour since

$\phi > 2$ are not expected due to the fast chemistry of hydrogen combustion and the enhanced mixing of micromix combustion system. From the values and the variation of these parameters it is possible to conclude that:

- Since $Le \sim 0.3$, the expected flame reactants diffuses around 3 times faster than its energy. This, added to the high laminar flame speed of H_2, creates a short flame with a thin flame front. However, flame front thickness also depends on the absolute value of the thermal diffusivity, so at low pressure it may increase and produce a short flame but slightly longer than at high pressure because of a thicker flame front. In addition, the high molecular diffusivity, compared to the thermal diffusivity, is likely to generate more unstable flames because the flame is supplied with fuel faster than its capability to evacuate the energy in the flame front.
- $Sc \sim 0.25$ in laminar flow means that H_2 to air mixing by diffusion is 4 times more significant than the capability of the injected H_2 to get the momentum that the air jet is transmitting to it. This has an effect on the penetration of H_2 in the air jet given a momentum-flux-ratio. However, the laminar value of Sc alone plays a minor role in cross-flow since mixing and momentum transport are enhanced by turbulence. It is necessary to estimate the turbulent Schmidt number to model the effective cross-flow mixing characteristics.

2 Flame regime characterization

Flame characteristics can be described by means of the Damköhler number (Da) and the Karlovitz number (Ka). The former relates the characteristic time of the turbulence integral scales (mixing) with the reaction time (2). High Da (> 1) means high reaction speed flames where mixing controls flame propagation. Although similar, the definition of the latter is related to turbulence-to-chemistry interaction. It is the ratio of the reaction time to the characteristics time of kolmogorov turbulent scale (length scale where the turbulence dissipates (3)). It can also be expressed as the flame thickness to kolmogorov scale. Low Ka (< 1) means the turbulence dissipates before being reduced to a size smaller than the flame thickness, therefore turbulence can not progress inside the flame front and it can be considered as a flamelet, i.e., a turbulent flame than can be considered as a differential set of laminar flames.

$$Da = \frac{\tau_t}{\tau_{ch}} = \frac{l_t\, s_l}{u'\, \delta_l} \tag{3}$$

$$Ka = \frac{\tau_{ch}}{\tau_\eta} = Da^{-1} Re_t^{1/2} \tag{4}$$

$$Re_t = \frac{u'\, l_t}{\nu} \tag{5}$$

Hydrogen-fuelled flames are expected to be characterized by high Da and low Ka since their laminar flame speed is higher than that of any conventional fuel (2 − 3 m/s). However, chemical, integral and kolmogorov time scales must be estimated to know what type of flame hydrogen-fuelled micromix flames are. The outcome of this analysis served to know what flame regime it is expected and what are the most suitable CFD combustion models that should approach the physical behaviour of these flames.

To estimate Da and Ka, the laminar flame thickness (δ_l), the laminar flame speed (S_l), integral turbulence scale (l_t), turbulent characteristic speed (u') and kinematic viscosity (ν) are needed. Among these parameters, viscosity is known from the correlations in previous section, integral turbulent scale is taken as the hydraulic diameter of the duct or air gate introducing the air into the combustion region and the turbulent characteristic speed is estimated as the 40% of the flow mean velocity ($30\ m/s$) from preliminary LES simulations. The laminar flame front is estimated using eq. (6) and the laminar flame speed obtained from Ravi et al. [5]. This correlation follows the form of eq. (7) and has an uncertainty of ±13 cm/s in the range of $T \in [270, 620]\ K$, $p \in [1, 30]\ atm$ and $\phi \in [0.5, 5]$.

$$\delta_l = 2\frac{\alpha}{S_l}\left(\frac{T_b}{T_u}\right)^{0.7} \tag{6}$$

$$S_l = [a_1 + a_2\phi + a_3\phi^2 + a_4\phi^3 + \ldots + a_5\phi^4]\left[T_u/T_{ref}\right]^{b_1+b_2\phi+b_3\phi^2+b_4\phi^3} \qquad T_{ref} = 320\ K \tag{7}$$

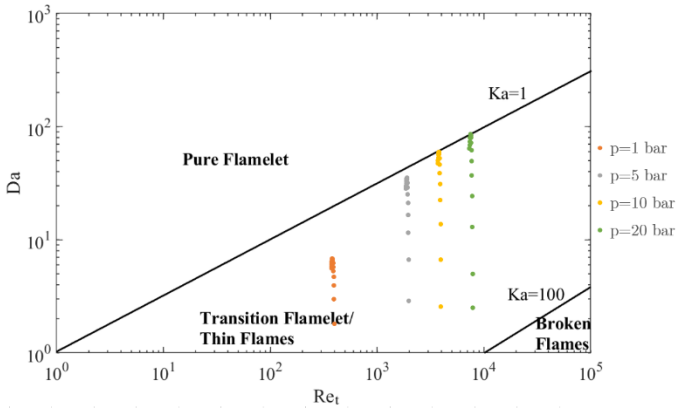

FIGURE 3: Non-premixed flame diagram. The plotted data corresponds to all the operating conditions where the hydrogen micromix combustor was simulated: $p \in (1, 5, 10, 20)\ bar$ and $\phi \in [0.5, 2]$ (diffusion flame) for $T_{air} = 600\ K$ and $T_{H_2} = 300\ K$.

In order to characterize flame regime for hydrogen micromix flames, the Borghi diagram is not suitable because it assumes $Le = Pr = Sc = 1$. In hydrogen flames, as it is explained in the previous section, the non-dimensional numbers differ significantly from 1. Furthermore, the line describing $Ka = 1$ in the Borghi diagram depends on pressure and equivalence ratio because how it is defined ($Ka = (\delta_l/\eta)^2$). Therefore, for different pressures and mixtures there would be several lines of $Ka = 1$ in a conventional Borghi diagram. In

order to classify the flame regime of hydrogen-fueled diffusion flames the non-premixed flame diagram is used (figure 3). In this diagram the effects of pressure and equivalence ratio are included in the Da and Re_t numbers. The definition of Ka in the non-premixed flame diagram is that in eq. (4) obtained from [28] and derived without any assumption on the Le, Sc or Pr numbers. Hence, the line of $Ka = 1$ is identical for any pressure and mixture.

This diagram consists of 3 different flame regimes depending on Ka and only considers fast chemistry compared to mixing ($Da > 1$), differently from Borghi diagram. In the first region, where $Ka < 1$, turbulent flames can be considered as a differential set of laminar flames (pure flamelet) because turbulence dissipates before entering the flame front. Here, the flames can be corrugated ($u'/S_l > 1$) or wrinkled ($u'/S_l < 1$). However, this diagram is not suitable to plot $u'/S_l = 1$ line to differentiate these two types of flamelets since on that line $Da = l_t/\delta_l = f(p, \phi)$. Therefore, this line would change with φ and p and it is impossible to ensure a point in the diagram where u'/Sl has an specific value.

In the second region, where $1 < Ka < 100$, the flamelet hypothesis still holds to solve the flames. It is a transition region from the pure-flamelet region and the broken flames region [29]. As Ka approaches the limit value of 100, the behaviour of the flames is more different from that of a flamelet and more error is produced by the flamelet hypothesis. This regime can also be called thin reaction flames.

The third region, where $Ka > 100$, turbulence can be much smaller than the flame front thickness. This allows eddies to progress inside the reaction zone and produce turbulent transport of radicals inside it, producing local quenching of the reactions and breaking the flame front. This regime is characterized by a strong turbulence-to-chemistry interaction and is called broken flames.

In a diffusion flame, it is expected to have a non-homogeneous mixture of fuel and air. That is why in figure 3 the flame non-dimensional numbers for different equivalence ratios are plotted to see the *range of regimes* that a diffusion flame could be defined by. Hydrogen-fueled micromix flames could be defined as transitional flamelets in the range of $1 < Ka < 100$. Particularly, relatively-high-ϕ points approach to $Ka = 1$ line, where the flamelet hypothesis does not deviate significantly from the actual flame regime. Since the flame found in micromix combustors is a diffusion flame, points with ϕ closer to the lower flammability limit are rare, therefore most of the flame is at $Ka \sim 1$, i.e., it is a transitional flamelet.

Da of hydrogen-fuelled flames in micromix combustion system is always bigger than 1 (figure 3). This means that chemistry is faster than mixing even though micromix system maximizes the mixing intensity through a cross-flow pattern. However, at points where ϕ is lean Da is close to 1 despite the fast chemistry of hydrogen flames, proving that mixing is maximized in micromix injectors.

From these data it is possible to conclude that the CFD flamelet model could be suitable for defining the flame behaviour while offering low computational cost as an extra feature of this model. The FGM Kinetic rate model implemented in STAR-CCM+ software also considers turbulence-chemistry interaction through the probability density functions (PDFs). With this, the possibility of local flame quenching due to turbulent species transport inside the flame front is accounted for. This potentially reduces the error of using the flamelet model in the transition regime since these phenomena that describe the transitional flamelet are included in the code. Following this line, using thickened flame model to predict turbulence-chemistry interaction together with flamelet model to generate combustion data could also be suitable. However, since Thickened flame model can only be used in LES simulations it can not be used to perform simulations in a short time.

In conclusion, the CFD combustion model that potentially best reproduces the expected flame physics with the lowest computational cost is the FGM Kinetic rate model in RANS simulations.

3 Calibration of Sc_t

Turbulence Schmidt number is used in RANS simulations to model the turbulent diffusivity of the flow field. Mixing is modelled by means of the sum of molecular and turbulent diffusivities, i.e., the effective diffusivity. In this case, even though H_2 molecular diffusivity is very high, the turbulent diffusivity of the flow field is even higher, thus controlling the mixing. Since Sc is fixed by the fluid properties, Sc_t must be calibrated according to the cross-flow field properties.

Before starting the calibration, it is important to note the following:

- The hypothesis of constant Sc_t in cross-flow is not true since it changes with the turbulence scale and the downstream distance to the injector and the wall distance [30]. A sensitivity analysis on this should be done.
- For non-reacting RANS simulations it has been observed that for jet-in-crossflow, a constant value of Sc_t should be around 0.2 [31]. This is for relatively small momentum flux ratio. However, the effect it has in downstream combustion has not been assessed.
- The Sc_t that was calibrated in this section is not the actual Sc_t but a numerical value to model the overall mixing behaviour. This is because RANS models tend to underestimate the turbulent viscosity, therefore Sc_t must be lower than in reality to reproduce a realistic turbulent diffusivity [31].
- Mixing in LES simulations is not controlled by the value of Sc_t but by the turbulent scales that are solved.

In order to calibrate the value of Sc_t, three RANS simulations were calculated with $Sc_t \in (0.1, 0.2, 0.7)$. RANS solution was averaged with the iterations since it was unstable. Then, a LES simulation was calculated and its results averaged in time for 8 flow-throughs across the flame. The results of

RANS and LES were compared based on the flame shape, temperature and emissions to finally get a constant value of Sc_t. A further study, once experimental results are generated, could include the variation of Sc_t along the flame.

3.1 Numerical setup

3.1.1 Geometry

A single injector/flame case was generated to perform all the preliminary simulations as well as the calibration of Sc_t and the evaluation of combustion models. This study was only performed in a single-injector combustor to capture the physics of a single flame.

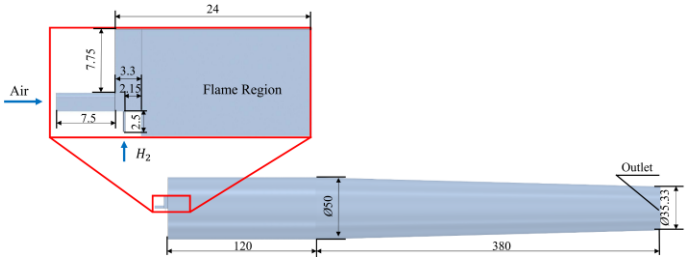

FIGURE 4: Single injector geometry.

3.1.2 Mesh

Three regions can be differentiated with different mesh size: the injector/flame region with base size of 0.125 mm, the intermediate pipe region with base size of 0.6 mm and the downstream pipe region with base size of 1 mm. The base size of the flame region was chosen through a mesh independence study. A base size of 1 mm provides enough resolution to capture the flow field in the pipe. Flame region dimensions were obtained from preliminary simulations. It was estimated a flame length of 20 mm for $p_0 = 20\ bar$, $T_{0\,air} = 600\ K$ and $T_{0\,H2} = 300\ K$, therefore the finest mesh region was set to 24 mm long from the injector wall.

The mesh size of the intermediate region is an intermediate value chosen arbitrary to ensure a smooth development of the flow field. Polyhedral mesh was used for the whole fluid domain. There is only wall refinement in the injector region (10 prism layers with a prism layer stretching of 1.1 and a prism layer thickness of 0.125 mm).

3.1.3 Physics models and boundary conditions

The physics models used in STAR-CCM+ version 13.06.014-R8 are:

- For RANS Steady: Steady, Three Dimensional, Turbulent, Reynolds-Averaged Navier-Stokes, K-Omega Turbulence, SST (Menter) K-Omega, Transition Boundary Distance, All y+ Wall Treatment. Most of these models are submodels of the K-Omega Tubulence model.
- For LES: Implicit Unsteady, Three Dimensional, Turbulent, Large Eddy Simulation, Exact Wall Distance, WALE Subgrid Scale and All y+ Wall Treatment.
- Fluid properties: Ideal Gas, Gradients, Multi-Component Gas, Segregated Flow and Segregated Fluid Enthalpy.
- Combustion: Reacting, Flamelet, Flamelet Generated Manifold (FGM), FGM Reaction and FGM Kinetic Rate
- NO_x emissions: NO_x Emission, NO_x Thermal and NO_x Zeldovich.

The boundary conditions are in table 1.

Boundary Condition	Parameter	Value
Air Inlet/Air gate (Mass flow inlet)	$\dot{m}_{air}$ [kg/s]	1.91E-3
	T_0 [K]	600
	Turbulence intensity [%]	5
	Turbulence scale [m]	1.83E-3
H_2 Inlet (Mass flow inlet)	$\dot{m}_{H_2}$ [kg/s]	2.41E-5
	T_0 [K]	300
	Turbulence intensity [%]	5
	Turbulence scale [m]	3E-4
Outlet (Pressure outlet)	Target mass flow rate [kg/s]	$\dot{m}_{air} + \dot{m}_{H_2}$
	Gauge pressure [bar]	0
Overall	ϕ	0.43
	Absolute p_0 [bar]	20

TABLE 1: Boundary conditions for the single injector geometry.

The fluid was modelled as an ideal gas. To generate the data for the flamelet model, 0D reactor was used and the chemistry mechanism used to define the reaction was that proposed by C. V. Naik and consists in 9 species and 25 reactions [32]. Kinetic rate was used to calculate reaction rate.

The unnormalized progress variable used to indicate the progress of the combustion is the mass fraction of water. Therefore, the (normalized) progress variable is 1 when the mass fraction of H_2O is maximum, i.e., when the combustion is completed.

The time step for LES simulations was 2 µs to ensure a Courant number close to 1 (from preliminary simulations it was estimated that residence time in the flame region ranges from 1.6 µs and 5 µs). Implicit unsteady solver was set to 2nd order. Each time step consisted on 20 iterations to ensure that all the residuals fall around 2 orders of magnitude within any time step.

3.2 Results and discussion

Figure 5 shows the evolution of the mass fraction of OH with the downstream distance in mm. The data displayed in this

figure was generated by averaging with the mass flow the mass fraction of OH in planes perpendicular to the flow direction spaced 0.25 mm.

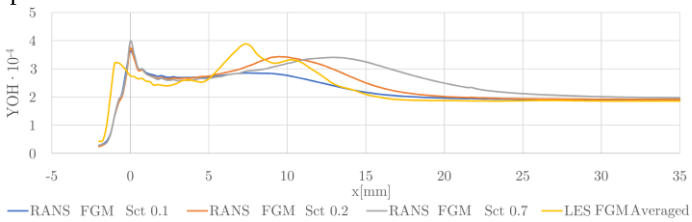

Figure 5: Evolution of the mass-flow averaged mass fraction of OH with downstream distance. $x = 0\ mm$ corresponds to the corner where the flame is attached as showed in figure 6.

According to figure 5, RANS simulation with $Sc_t = 0.1$ predicts the shortest flame followed by LES, RANS with $Sc_t = 0.2$ and RANS with $Sc_t = 0.7$. This is because a lower Sc_t means a higher turbulent diffusivity, i.e., species are transported much faster than momentum. Faster species transport means they mix in a shorter distance, thus displacing the reaction zone upstream. In addition, due to the high diffusion in the low Sc_t simulation, some H_2 diffuses fast enough into the jet of air that it mixes out of its lower flammability limit. This mainly happens in the reacting region at the center of the jet of air (see figure 6). There, the mass fraction of OH is lower if $Sc_t = 0.1$ because some of the H_2 is not entering that reaction region. Due to this phenomenon the maximum mass fraction of OH when $Sc_t = 0.1$ is the lowest in figure 5. In contrast, the evolution Y_{OH} when $Sc_t = 0.7$ is produced by poorer mixing and a longer reaction region compared to $Sc_t = 0.1$.

The evolution of the mass fraction of OH predicted by the LES simulation is in between the evolution predicted by $Sc_t = 0.1$ and $Sc_t = 0.2$. This is indicative that a turbulent Schmidt number in the range $Sc_t \in [0.1, 0.2]$ should be able to model the mixing characteristics of cross-flow in such a way that it approaches LES results even more than 0.1 or 0.2.

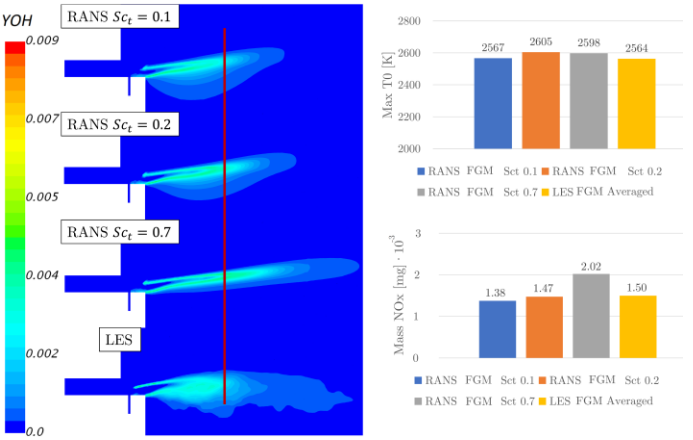

FIGURE 6: Single injector symmetry plane: on the left, the contours of the mass fraction of OH are displayed. The red line is used to compare the flame length predicted by LES to the rest of solutions. On the right, the maximum total temperature and the mass of NO_x in the flame region for different simulations is showed.

The above discussion is supported by the contours of Y_{OH} in figure 6. The red line shows the predicted flame length by the LES solution, corresponding arbitrarily to $Y_{OH} = 0.25$ where the total temperature starts to fall significantly (this choice is performed since Y_{OH} gradients cannot be easily extracted from CFD simulations). In these contours it is possible to see how $Sc_t = 0.1$ produces a slightly-shorter flame and $Sc_t = 0.2$ a slightly-longer flame than LES. In addition, both $Sc_t = 0.1$ and $Sc_t = 0.2$ simulations predict the downward flame propagation showed in LES contours while $Sc_t = 0.7$ simulation does not.

Interestingly, all the calculated flames are attached to the corner of the wall as can be deduced from figure 5 at $x \in [-2, 0]$ mm, where Y_{OH} increases to its first peak. This implies that combustion in this zone is not due to how turbulence is solved but to the combustion model. The combustion in the region between the H2 injector and the corner is produced because of the low local velocities induced by the cross-flow pattern. This creates a zone where the equivalence ratio is high and the velocity is low. In this case, depending on how the combustion model predicts flame propagation, this region may or may not be burning. Therefore, it is possible that FGM kinetic rate combustion model is overpredicting flame propagation and the wall does not actually burn.

Maximum temperature also depends on mixing (figure 6). In this case, $Sc_t = 0.1$ produces the closest-to-LES maximum total temperature. Maximum total temperature is produced in the wall where the flame is attached (figure 5 at $x \in [-2, 0]\ mm$). It is expected that greater turbulent diffusion ($Sc_t = 0.1$) produces lower H_2 concentrations in the near-to-H_2-jet region. This implies that the turbulent diffusivity predicted with $Sc_t = 0.1$ is closer to that in LES simulations in this region. As explained at the beginning of this section Sc_t is not actually constant.

Mass of NO_x showed in figure 6 is the averaged mass of NO_x produced in the numerical region that contains the flame. This parameter has no technological application but it allows to qualitatively describe the effect of residence time and flame temperature on NO_x production in the flame. Since emissions trends were calculated in the final simulations, it was necessary to include NO_x production in the calibration process.

The flame predicted through RANS simulation with $Sc_t = 0.2$ produces slightly-lower NO_x than LES simulations while RANS simulations with $Sc_t = 0.1$ and with $Sc_t = 0.7$ produce respectively much lower and much higher NO_x. NO_x production depends mainly on residence time (flame length) and flame temperatures. In the steady RANS simulations with different Sc_t the temperature along the flame is very similar, so the controlling parameter for NO_x production is the residence time. This explains why $Sc_t = 0.1$ simulation shows the lowest mass of NO_x and $Sc_t = 0.7$ the highest. However, this simple analysis can not be applied to LES time-averaged results (figure 6) since the instantaneous flame temperatures are higher than the average, thus producing higher NO_x (figure 7).

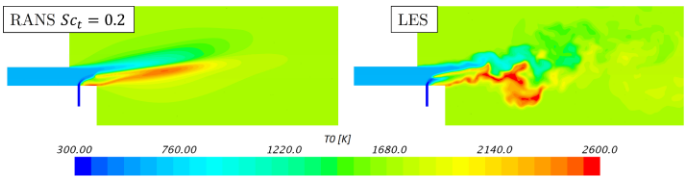

FIGURE 7: Single injector symmetry plane: contours of total temperature of steady RANS with $Sc_t = 0.2$ and LES in a random time step.

In LES, the higher instantaneous temperatures together with the thicker flame make that NO_x prediction is even higher than that of steady RANS with $Sc_t = 0.2$ where averaged temperatures are higher and the flame longer (compared to LES averaged). Therefore, it is possible to conclude that to approach NO_x prediction of RANS simulations to that of LES the turbulent Schmidt number should be slightly higher than 0.2.

From this analysis, it is possible to conclude that $Sc_t = 0.2$ is a good compromise between flame length and emissions production. However, it is important not to forget that in actual flames the turbulent Schmidt number is higher and not constant. In the future, a model describing the variation of Sc_t along the flame would be useful to match simulation to experimental data.

4 Combustion models comparison

In this section, three different simulations were compared. Two of them have the same combustion model (FGM kinetic rate) but different turbulence model (LES and k-ω RANS) while the third one was simulated with Thickened flame model that can only be LES. The aim of this section was to analyse and compare the flame structure and NO_x emissions that the most suitable combustion models (according to the predicted flame regime) can predict. This will be helpful when the ENABLEH2 team at Cranfield University carries out experiments in a hydrogen micromix combustor to be aware of different modelling possibilities of STAR-CCM+ and, if possible, calibrate them to be validated.

4.1 Numerical setup

The geometry, mesh and physics models are mostly the same as in the previous section. There are two main differences in the CFD set up. First, the combustion model was changed from FGM kinetic rate to Thickened flame model. Second, since the flame propagation rate in the Thickened flame model is given by the laminar flame speed, the correlation in [5] was extended with the experimental data at 10 bar and $\phi = 0.3$ in [33] and expressed as a function of the mixture fraction (7). Due to the low variation with pressure of laminar flame speed at $\phi = 0.3$, it was assumed to be similar at 10 bar and 20 bar.

$$S_l = a_0 + a_1 Z + a_2 Z^2 + a_3 Z^3 + a_4 Z^4 \qquad (8)$$

Coefficient	$\phi \in [0.3, 2]$	$\phi \in [2, 5]$
a_0	2.54	5.89
a_1	-602.47	70.04
a_2	44190	-1524.4
a_3	-920309	5736.8
a_4	6136105	0

TABLE 2: Coefficients for the modified laminar flame speed correlation for 20 bar, eq. (8).

4.2 Results and discussion

Contours of Y_{OH} and T_0 (figure 8) show that all the combustion models predict flame attachment to the corner of the wall. However, Thickened flame model shows lower temperatures in the wall region than FGM Kinetic rate. This is because each model has a different propagation mechanism. In the case of Thickened flame, the reaction propagates according to the laminar flame speed (based on experimental data) and the turbulence-chemistry interaction while in FGM Kinetic rate it is computed from the reaction kinetics and the turbulence-chemistry interaction. Since flame attachment to the wall is predicted by these two models, it means it does not depend on the combustion model and should be further studied in the future. This analysis is important because the high local temperature near the wall may lead to a decrease in the life of the combustor injector plate. For future work to increase the life of hydrogen micromix combustor, a thermal analysis must be performed, the geometry could be redesigned or the inclusion of a heat shield protecting the wall studied.

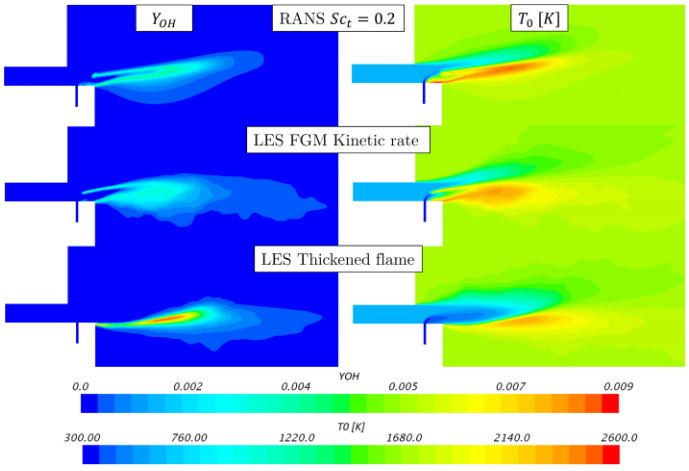

FIGURE 8: Single injector symmetry plane: on the left, the contours of the mass fraction of OH are displayed showing different flame length and thickness. On the right, the contours of total temperature are showed. LES contours are averaged.

The flame structure calculated with the thickened flame model is entirely in the region where the mixed jet is interacting with the vortexes produced between the jet and the walls. Here, the velocity of the fluid is the lowest and the residence time is increased, thus allowing the reaction to start. Higher residence

time in the flame front increases OH and NO_x production. This explains that Thickened flame model predicts higher Y_{OH} locally and that, despite the lower total temperatures in the flame, the NO_x production is similar compared to FGM Kinetic rate results.

In contrast, the flame predicted by FGM Kinetic rate is in the middle of the jet, where the velocity of the fluid is maximum. This implies that there is a noticeable difference in the flame structure when different flame propagation models are used. In the case of FGM Kinetic rate, flame propagation is fast enough to anchor the flame in a high-speed region while in Thickened flame it is slower and can only anchor the flame to the low-speed zone. Consequently, and due to the lack of experimental data, it is uncertain where the flame actually starts.

The maximum total temperature and the mass of NO_x in the flame region are lower with Thickened flame model than with FGM Kinetic rate in RANS and LES. The maximum total temperature is lower because the flame propagation is slower in the thickened flame model. This causes that the flame is not attached to the wall between the corner and the H_2 injector, where the maximum temperatures are produced, and thickens the flame. A thicker flame means that the thermal diffusivity is high enough to spread the reaction region and evacuate some energy out of it. Since the reaction is produced progressively in a wider space the temperature in the flame front is lower. Finally, Thickened flame model virtually thickens the flame front to solve the turbulence-chemistry interaction inside it. According to the flame regime of hydrogen micromix flames (figure 3) there may be species transport inside the flame front, thus creating local zones poor in H_2 or H^+ radicals where the reaction is quenched. Therefore, the more detailed resolution of the flame front inner structure could also be responsible for the lower temperatures in the thickened flame model.

Regarding NO_x production, it is important to note again that in LES it is a time-averaged value that depends on the instantaneous local temperatures along the flame. Since flame propagation in Thickened flame model is slower, overall residence time is increased. However, the fact of thickened flame model producing lower NO_x means that instantaneous local temperatures are much lower than in RANS and LES with FGM Kinetic rate, where the residence time is lower. These two flame characteristics compensate each other resulting in a very similar NO_x production.

Finally, among these two combustion models, FGM kinetic rate seems a more promising option to run hydrogen micromix CFD simulations because it can use RANS solvers, thus minimizing the computational cost, and because its flame propagation rate is not based on laminar flame speed, whose behavior at high pressure is not experimentally documented at $p > 10\ bar$.

CONCLUSION

Along this paper a methodology to estimate the physical properties of H_2, air and H_2-air mixtures was given for a range of temperature, pressure and equivalence ratio. For the leanest equivalence ratio (0.3), where minimum NO_x was expected, the Schmidt, Lewis and Prandtl numbers were estimated as 0.22, 0.35 and 0.75 respectively.

It was concluded that the conventional Borghi diagram is not suitable to characterize the flame regime of hydrogen micromix diffusion flames because it assumed $Sc = Le = Pr = 1$ and is only for premixed flames. The non-premixed flame diagram was defined and used to determine that hydrogen micromix flames are transition flamelets. From this analysis, FGM kinetic rate and Thickened flame combustion models were chosen as appropriate to reproduce the physics of the transitional flamelet flame regime.

Turbulent Schmidt number for cross-flow combustion was set to 0.2 as a compromise between accuracy on NO_x and flame length prediction. RANS and LES simulations of a single micromix injector were compared to calibrate this parameter. If Sc_t is higher than 0.2, NO_x production in RANS would be more similar to that in LES. In contrast, if it is lower than 0.2, the flame length in RANS would be more similar to that in LES. If this parameter is calibrated for a single flame, it should also be calibrated for multiple flames because flame-interaction between different injectors depends on mixing, which is equally dependent on Sc_t for both simulations. A sensitivity analysis could be done for multiple-injector configuration.

Finally, FGM kinetic rate and Thickened flame combustion models were compared in a single hydrogen micromix flame. It was concluded that flame structure and temperature distribution along the flame change significantly depending on the combustion and turbulence models. Flame attachment to the wall only depends on the flame propagation predicted by each combustion model. This phenomenon and its implication should be further studied by means of a heat transfer analysis. The addition of a heat shield to protect the wall against high temperature should be considered. Thickened flame model predicts lower maximum total temperatures and higher residence time than FGM Kinetic rate because the flame is developed in a low-speed region. These two phenomena compensate each other resulting in a similar production of NOx in the flame region.

ACKNOWLEDGEMENTS

The ENABLEH2 Project is receiving funding from the European Union's Horizon 2020 research and innovation programme under grant agreement Nº 769241.

REFERENCES

[1] P. Argüelles, J. Lumsden, M. Bischoff, D. Ranque, P. Busquin, S. Rasmussen, B.A.C. Droste, P. Reutlinger, R. Evans, R. Robins, W. Kröll, H. Terho, J. L. Lagardère, A. Wittlöv, and A. Lina. *European Aeronautics: A VISION for 2020*, 2001. European Commission, Luxembourg, 2001. ISBN 92-894-0559-7.

[2] Advisory Council for Aeronautics Research in Europe (ACARE). *Flightpath 2050*, page 28, 2011. ISBN: 978-92-79-19724-6.doi: 10.2777/50266. URL

http://www.acare4europe.com/sria/flightpath-2050-goals/protecting-environment-and-energy-supply-0.

[3] M. Cames, J. Graichen, A. Siemons, and V. Cook. *Emission Reduction Targets for International Aviation and Shipping*. European Parliament - Policy Department, (1): 1–52, 2015. URL https://www.europarl.europa.eu/RegData/etudes/STUD/2015/569964/IPOL_STU(2015)569964_EN.pdf

[4] A. Murphy. *Aviation emissions and the Paris Agreement*. 8(January):1–4, 2016.

[5] S. Ravi and E. L. Petersen. *Laminar flame speed correlations for pure-hydrogen and high-hydrogen content syngas blends with various diluents*. International Journal of Hydrogen Energy, 37(24):19177–19189, 2012. ISSN 03603199. doi: 10.1016/j.ijhydene.2012.09.086.

[6] D. Cecere, E. Giacomazzi, and A. Ingenito. *A review on hydrogen industrial aerospace applications*. International Journal of Hydrogen Energy, 39(20):10731–10747, 2014. ISSN 03603199. doi: 10.1016/j.ijhydene.2014.04.126. URL http://dx.doi.org/10. 1016/j.ijhydene.2014.04.126.

[7] A. Lanz, J. Heffel, and C. Messer. *Hydrogen Fuel Cell Engines and Related Technologies*. Fuel Cell Technology, page 53, 2001. doi: 10.1007/ 1-84628-207-1

[8] G. Dahl. *Engine control and low-NOx combustion for hydrogen fuelled aircraft gas turbines*. International Journal of Hydrogen Energy, 23(8):695–704, 2002. ISSN 03603199. doi: 10.1016/s0360-3199(97)00115-8.

[9] European Comission. *ENABLing cryogEnic Hydrogen based CO2 free air transport (ENABLEH2)*, 2018. URL https://cordis.europa.eu/project/rcn/216008/en

[10] NASA. *Technology Readiness Level*, 2012. URL https://www.nasa.gov/directorates/heo/scan/engineering/technology/txt_accordion1.html.

[11] G. M. Ottino, A. Fancello, M. Falcone, R. J.M. Bastiaans, and L. P.H. De Goey. Combustion Modeling Including Heat Loss Using Flamelet Generated Manifolds: A Validation Study in OpenFOAM. Flow, Turbulence and Combustion, 96(3):773–800, 2016. ISSN 15731987. doi: 10.1007/s10494-015-9666-5. URL http://dx.doi.org/10.1007/s10494-015-9666-5.

[12] J. A. Van Oijen, A. Donini, R. J.M. Bastiaans, J. H.M. ten Thije Boonkkamp, and L. P.H. de Goey. *State-of-the-art in premixed combustion modeling using flamelet generated manifolds*. Progress in Energy and Combustion Science, 57:30–74, 2016. ISSN 03601285. doi: 10.1016/j.pecs.2016.07.001. URL http://dx.doi.org/10.1016/j.pecs.2016.07.001.

[13] P. Yeung, S. Girimaji, and S. Pope. *Straining and Scalar Dissipation on Material Surfaces in Turbulence*. Combustion and Flame, 365(79):340–365, 1990.

[14] W. J. S. Ramaekers, B. A. Albrecht, J. A. Van Oijen, L. P. H. de Goey, and R. G. L. M. Eggels. *The Application of Flamelet Generated Manifolds in Modelling of Turbulent Partially-Premixed Flames*. Proceedings of the Fluent Benelux User Group Meeting, (November 2014):16, 2005. URL https://research.tue.nl/en/publications/the-application-of-flamelet-generated-manifolds-in-partailly-prem.

[15] G. M. Ottino, A. Fancello, M. Falcone, R. J.M. Bastiaans, and L. P.H. De Goey. *Combustion Modeling Including Heat Loss Using Flamelet Generated Manifolds: A Validation Study in OpenFOAM*. Flow, Turbulence and Combustion, 96(3):773–800, 2016. ISSN 15731987. doi: 10.1007/s10494-015-9666-5. URL http://dx.doi.org/10.1007/s10494-015-9666-5.

[16] R. J.M. Bastiaans, A. W. Vreman, and H. Pitsch. *DNS of lean hydrogen combustion with flamelet-generated manifolds*. Center for Turbulence Research Annual Research Briefs, 28(1983):195–206, 2007.

[17] O. Colin, F. Ducros, D. Veynante, and T. Poinsot. *A thickened flame model for large eddy simulations of turbulent premixed combustion*. Physics of Fluids, 12(7): 1843–1863, 2000. ISSN 10706631. doi: 10.1063/1.870436.

[18] W. Han, H. Wang, G. Kuenne, E. R. Hawkes, J. H. Chen, J. Janicka, and C. Hasse. *Large eddy simulation/dynamic thickened flame modeling of a high Karlovitz number turbulent premixed jet flame*. Proceedings of the Combustion Institute, 37(2):2555–2563, 2019. ISSN 15407489. doi: 10.1016/j.proci.2018.06.228. URL https://doi.org/10.1016/j.proci.2018.06.228.

[19] E. W. Lemmon and R. T. Jacobsen. *Viscosity and Thermal Conductivity Equations for Nitrogen, Oxygen, Argon, and Air*. International Journal of Thermophysics, 25(1), 2004.

[20] E. N. Yusibani, P. L. Woodfield, Y. Takata, and M. Fujii. *Prediction of Hydrogen Gas Viscosity at High Pressure and High Temperature*. pages 21–27.

[21] S. Perry, R. H. Perry, D. W. Green, and J. O. Maloney. *Chemical Eengineer' Handbook*. McGraw-Hill, 7th edition, 1997. ISBN 0070498415.

[22] E. W. Lemmon, M. L. Huber, and J. W. Leachman. *Revised Standardized Equation for Hydrogen Gas Densities for Hydrogen Gas Densities for Fuel Consumption Applications*. 113(6):341–350, 2008.

[23] M. J. Assael, J. A. M. Assael, M. L. Huber, R. A. Perkins, and Y. Takata. *Correlation of the Thermal Conductivity of Normal and Parahydrogen from the Triple Point to 1000 K and up to 100 MPa).* 033101 (May 2016), 2014. doi: 10.1063/1.3606499.

[24] S. R. Turns. *An Introduction to Combustion Concepts and Applications. McGrawHill*, second edition, 2000. ISBN 0-07-230096-5.

25

] W. He, W. Lv, and J. Dickerson. *Gas Transport in Solid Oxide Fuel Cells. Chapter 2: Gas Diffusion Mechanisms and Models*. Springer, 2014. ISBN 9783319097374. doi: 10.1007/978-3-319-09737-4.

[26] N. Matsunaga, M. Hori, and A. Nagashima. *Measurement of Mutual Diffusion Coefficients of Gases by the Taylor Method: Measurements on H_2-Air, H_2-N_2, and H_2-O_2 Systems*. Heat Transfer - Asian Research, 31(3):182–193, 2002. doi: 10.1002/htj.10025.

[27] C. R. Wilke. *A Viscosity Equation for Gas Mixtures*. 517(1950):20–23, 1969. doi: 10.1063/1.1747673.

[28] N. Peters. *Laminar Flamelet Concepts in Turbulent Combustion*. pages 1231–1250, 1986.

[29] N. Peters. Turbulent Combustion. Cambridge University Press, Cambridge, 2000.

[30] A. T. Wassel and I. Catton. *Calculation of turbulent boundary layers over flat plates with different phenomenological theories of turbulence and variable turbulent Prandtl number*. International Journal of Heat Mass Transfer, 16:1547–1563, 1973.

[31] Y. Tominaga and T. Stathopoulos. *Turbulent Schmidt numbers for CFD analysis with various types of flow field*. 41:8091–8099, 2007. doi: 10.1016/j.atmosenv.2007.06.054.

[32] C. V. Naik, K. V. Puduppakkam, and E. Meeks. *An Improved Core Reaction Mechanism for Saturated C0-C4 fuels*. 134(February 2012):1–15, 2012. doi: 10.1115/1.4004388.

[33] D. Bradley, M. Lawes, K. Liu, S. Verhelst, and R. Woolley. *[* 149:162–172, 2007. doi: 10.1016/j.combustflame.2006.12.002.

Characterising hydrogen micromix flames: combustion model calibration and evaluation

López-Juárez, Marcos

2021-01-11

López-Juárez M, Sun X, Sethi B, et al., (2021) Characterising hydrogen micromix flames: combustion model calibration and evaluation. In: ASME TurboExpo 2020, 21-25 September 2020, London, Virtual Event. Paper number GT2020-14893

https://doi.org/10.1115/GT2020-14893